RSC Advances




ROYAL SOCIETY OF CHEMISTRY

www.rsc.org/advances

# Chemically grafted graphite nanosheets dispersed in poly(ethylene-glycol) by γ-radiolysis for enhanced lubrication

Bhavana Gupta [a], Kalpataru Panda [b], Niranjan Kumar [a]*, Ambrose A. Melvin [c], Sitaram Dash [a], Ashok Kumar Tyagi [a]

[a]Materials Science Group, Indira Gandhi Centre for Atomic Research, Kalpakkam, India

[b]Graduate School of Engineering, Osaka University, Osaka, Japan

[c]Catalysis Division, CSIR-National Chemical Laboratory, Dr. Homi Bhabha Road, Pune, India

## Abstract

Graphite nanosheets (Gr-NS) dispersed in poly(ethylene-glycol) (PEG200) medium was subjected to various doses of γ-irradiation. Hydroxyl functional group present in PEG is chemically grafted through hydrogen bonding with hydroxyl, carbonyl and carboxylic groups of Gr-NS. Grafting process is driven by the generation of active radicals from solvent radiolysis. Chemical grafting was investigated by X-ray photo electron spectroscopy (XPS) and Fourier transform infra-red spectroscopy (FTIR). The result of spectroscopic studies revealed reduction in oxygen functionality in PEG-Gr-NS at higher dose of γ-irradiation. The γ-irradiation not only bridges the functionalities between PEG and PEG-Gr-NS but edge and basal plane defects in Gr-NS are further reduced as evident from Raman analysis. Inter-planer sheet distance in Gr-NS is increased due to intercalated chemical grafting with PEG molecules. The chemical grafting between PEG and Gr-NS and reduction in defect enhances tribological properties with decrease in 26% and 32% of friction coefficient and wear, respectively as compared to PEG alone. Lubrication mechanism is mediated through inter-planer weak forces when PEG is chemically grafted with Gr-NS. The electrostatic interaction of PEG with Gr-NS acts as a molecular bridge thus enhancing sustainability of tribo-stress. Additionally, in the presence of functionalized PEG-Gr-NS tribo-contact condition, the evidence of deposited graphitic tribo-film was observed from micro-Raman spectroscopy inside the steel wear track. This film further enhanced lubrication mediated through low shear strength interlayer graphite sheets and therefore, antiwear properties are synergistically improved.


**Keywords:** Graphite nanosheet, γ–radiolysis, Friction, Lubrication

## 1 Introduction

In the modern days, the effective utilization of energy efficient techniques is required due to continuous increase in greenhouse gas emissions and the depletion of the fossil fuels. Usually, in passenger cars, the direct frictional losses, excluding the braking friction, are estimated to consume 28% of the fuel energy.[1] Reduction of friction in mechanical systems is one of the most important ways for improving energy efficiency of the machine components and maintain clean environment. Depending upon contact pressure, there are several solid, liquid and gaseous lubricants which act effectively to reduce friction and wear. In microscopic scale, lubrication of carbon nanotubes and fullerene shows wear free motion anticipated by weak van der Waals force acting between the interlayer of walls and translational/rotational motion accomplished by fullerene moieties acting as spring and nanobearings.[2–4] On the other hand, graphite, graphene and other lamellar solids such as crystalline molybdenum disulphide ($MoS_2$) and tungsten disulphide ($WS_2$) are known to be good solid lubricants and, thus, are widely used in several practical applications. These layered lamellar structures are analogous to stacked non-adherent lattices which easily slip while applying tangential forces, thereby yielding ultra-low friction coefficient.[5–9] Usage of these lamellar materials is promising for engine lube additives required for direct energy saving applications. This is possible, if liquid lubricant is chemically grafted with lamellar materials via functionalization which allow shear and high strength boundary film formation on sliding interfaces.[10,11] Several engineering requirement like mechanical strength, load bearing capacity and shear stability of sliding interfaces are easily achieved by using nanostructured layered materials dispersed in the lube oils. However, dispersion of nanomaterials in the lube medium is challenging due to the difference in cohesive forces. But high specific surface area of lamellar materials enhances ability towards chemical functionalization and better dispersibility in lube medium. There are several reports which show functionalized graphene as a

compatible lube additive to be used as friction reducing agent via weak shear forces acting between the lamellar sheets. This effect is realized when graphene is chemically grafted with lube component.[6,12–15] Functionalization and chemical grafting of carbon materials with hydrocarbon based lubricant is favorable compared to other lamellar materials due to molecular similarity which allows easy chemical bridging. It is reported that uniform dispersion of graphite nanosheets in the base oil is effective if –OH and –COOH groups are introduced during the sheet preparation.[12,16] A functionalization with long chain compounds i.e., aliphatic amine to obtain the amide derivative enhances their dispersibility in nonpolar solvents. On the other hand, polarity increases in functionalized nanosheet, and it can be dispersed through the use of a dispersant avoiding further chemical reaction. This makes carbon a robust and technically suitable material for synthesizing lube based friction reducing additives. It is reported that dispersed graphene additives in the lube medium significantly reduces friction and wear of the sliding interfaces.[6,10–12,14] However, enhanced lubrication properties of this material are restricted only to smooth contact interfaces due to low–dimensional order (2D) of graphene,. The thinner sheets of graphene stick and further penetrate to the metal subsurface of the sliding contacts due to plastic deformation and limit their sustainability required to provide long term lubrication mechanism. To overcome these above problems, the dispersion of functionalized graphite nanosheets possibly restrict subsurface penetration due to their larger dimension (3D). It is possible to provide direct lubrication in rough contact when the thickness of the graphite sheet becomes larger than the contact asperities. In one hand, solid lubrication properties of graphite in micro and macroscopic scale are well studied and it is understood that low friction behavior in this material is governed by weak van der Waals interlayer forces, passivation of dangling bonds and presence of incommensurate sliding interfaces.[5,17–21] Unfortunately, less research has been

carried out to understand the lubrication mechanism of freely suspended graphite nanosheets (Gr-NS) as compared to graphene based lube additives. It is understood that preparation of graphene requires chemical processing which generates unwanted harmful chemical waste for environment. However, graphite nanosheets can be prepared and functionalized without releasing unwanted chemical waste.

For the first time, we propose direct dispersion and functionalization of commercial grade graphite nanosheets (Gr-NS) in poly(ethylene-glycol) (PEG200) applying γ-irradiation dose. This is environmentally clean and facile approach to produce graphite nanosheets for friction and wear reducing additives in lube medium. It is proposed that oxygen functionalization of Gr-NS is grafted by the hydrogen bonding with hydroxyl group of intercalated PEG molecules. The PEG-Gr-NS is characterized by X-ray photo electron spectroscopy (XPS), furrier transform infra-red spectroscopy (FTIR), Raman spectroscopy and high resolution transmission electron microscopy (HR-TEM). Evidence of lubrication mechanism due to the presence of Gr-NS tribo-film in the wear track is characterized by micro-Raman spectroscopy. Wear tracks dimension, morphology and chemical behavior was investigated to observe the effect of lubrication.

## 2 Experimental

### 2.1 Material synthesis

Standard commercial grade graphite was obtained from Sigma Aldrich. Prior to γ-ray treatment, graphite powder (weight 30 mg) in 3 ml PEG200 was dispersed by ultrasonication, working at frequency 30 kHz for 3 hours. The γ- irradiation is effective when volume of the material is less. In this condition, the dose of irradiation is homogenously distributed all around the sample. PEG is a promising solid–liquid organic phase change materials because of its high phase change enthalpy, chemical stability and suitable melting temperature which can be tuned by its molecular weight.[22,23] Nitrogen purging was carried out for 5 minutes to remove dissolved

oxygen content. The resultant dispersion of graphite (weight 30 mg) in 3 ml PEG200 was then irradiated in a γ-ray chamber which housed a $^{60}$Co γ-ray source for 0, 18, 36 and 54 hours (h) at a dose rate 5.1 KGy $h^{-1}$ under atmospheric sealed condition. After completion of reaction, glass vial colour changed to brown and the dark blackish colour dispersed PEG200 functionalized graphite powder was collected. This was processed after centrifugation, washed in water and dried in a vacuum oven at 60$^{o}$C for obtaining powder form of PEG200 functionalized Gr-NS. The dose dependent irradiation effect on the PEG-Gr-NS was investigated using various techniques. The procedure is a green and facile approach to synthesize and functionalize Gr-NS hybrid material for tribology application. In this process, PEG200 solvent undergoes high-energy γ-irradiation resulting in the formation of ions, excited molecules, electrons and radicals. The electrons can easily get further solvated with PEG solvent molecules. The highly reducing activated electrons or solvated electrons are responsible for the reduction of oxygen functionality[24] and therefore, PEG radicals react with Gr-NS leading to functionalization through hydrogen bonding. For simplicity, the sample with γ-ray exposure of 0, 18, 36 and 54 h will be here after designated by PEG-Gr-$NS_0$, PEG-Gr-$NS_1$, PEG-Gr-$NS_2$ and PEG-Gr-$NS_3$, respectively, throughout the manuscript. The PEG-Gr-$NS_0$ sample is pristine and non-irradiated one.

### 2.2 Characterization of hybrid PEG-Gr-NS

Morphology and microstructure of PEG-Gr-NS were analyzed by field emission scanning electron microscope (FESEM, Zeiss Supra 55) and HR-TEM. Powder X-ray diffraction (XRD) measurements were carried out using PANalytical X'pert Pro dual goniometer consists of Cu Kα (λ= 0.15418 nm) rotating anode to investigate crystallography of PEG-Gr-NS samples. Chemical bonding feature were investigated by XPS (ULVAC-Phi ESCA1800) using a monochromatic

MgKα source operated at 400 W and 1253.6 eV. Chemical structure of samples including with wear tracks analysis was carried out by micro-Raman spectrometer (Ranishaw) operating in laser wavelength of 514.5 nm. FTIR spectrometer (Bruker Optics), operating in transmission mode, spectral resolution 4 $cm^{-1}$ was used for the functional analysis of PEG and PEG-Gr-NS samples. This analysis was also carried out on buried PEG-Gr-NS dispersed in PEG which was collected from the wear track after the tribology test. Wear track dimension and morphology was characterized by optical microscope and FE-SEM. PEG200 was used as synthetic lube base oil for tribology evaluation of PEG-Gr-NS hybrid nanomaterials. PEG200 functionalized powder nanographite sheet i.e. abbreviated by PEG-Gr-NS was thoroughly dispersed in the PEG200 by ultrasonification process and their dispersion stability was monitored for 3 days. Ultrasonication was carried out for 3 hours at frequency 30 kHz for the dispersion of powder PEG-Gr-NS in PEG200 lube medium. Dispersion time was optimized at constant frequency of 30 kHz. It was visibly observed that for less than 1 hour the dispersion of the Gr-NS was not stable and particle was agglomerated after 1 day. However, when ultrasonication time was more than 1 hour, the agglomeration was absent and PEG200 functionalized Gr-NS was homogeneously distributed in PEG200 medium. The tribo-evaluation of PEG200 dispersed PEG-Gr-NS was carried out by measuring friction and wear properties using ball-on-disc standard tribometer (CSM Instrument, Switzerland) operating in linear reciprocating mode. A 100Cr6 spherical steel ball with diameter 6 mm was used as a sliding material against the stationary lubricated steel (316LN) disc. The sliding ball was mounted in a holder, which was connected through a stiff lever coupled with the friction force transducer. The friction coefficient was determined by linear variable differential transformer (LVDT) sensor measuring the deflection in the elastic arm. All experiments were carried out at constant normal load of 1 N, linear sliding speed of 3 cm/s, stroke length of 4 mm

and sliding distance of 100 meters. In each tribo-test, two drops of PEG-Gr-NS dispersed in PEG200 lubricant was used which thoroughly lubricated the sliding interfaces. In-situ wear depth was measured by LVDT sensor coupled to the core of a tribometer. All tribo-tests were carried out in ambient environment.

## 3 Results and discussion

### 3.1 XRD, FE-SEM and HR-TEM analysis of PEG-Gr-NS

XRD analysis was used to characterize the crystalline nature and phase purity of the Gr-NS samples. PEG-Gr-$NS_0$ shows a diffraction peak of (002) plane at 26.62$^o$ 2θ which is shifted to low 2θ in PEG-Gr-$NS_3$ which clearly indicates increase in interlayer spacing after the γ–radiolysis (Fig. 1). FWHM of (002) peak is reduced in PEG-Gr-$NS_3$ sample, specifying increase in thickness of the graphite sheets along the c-axis. This value is 5.3 nm in PEG-Gr-$NS_0$ and increased to 8.93 nm in PEG-Gr-$NS_3$ sample. The thickness of the PEG-Gr-NS is calculated by Scherrer equation:

$$d = \frac{K\lambda}{\beta \cos\theta}$$

where $d$ is the mean size of crystalline graphite domains, $K$ is a dimensionless shape factor with a value close to unity, $\lambda$ is the X-ray wavelength, $\beta$ is the line broadening and the $\theta$ is the Bragg angle. Above analysis clearly points to increase in not only interlayer spacing but also increase in number of sheets in graphite that could be driven by γ–radiolysis. In both the samples, the XRD results are produced in three different locations and the characteristic was nearly similar.

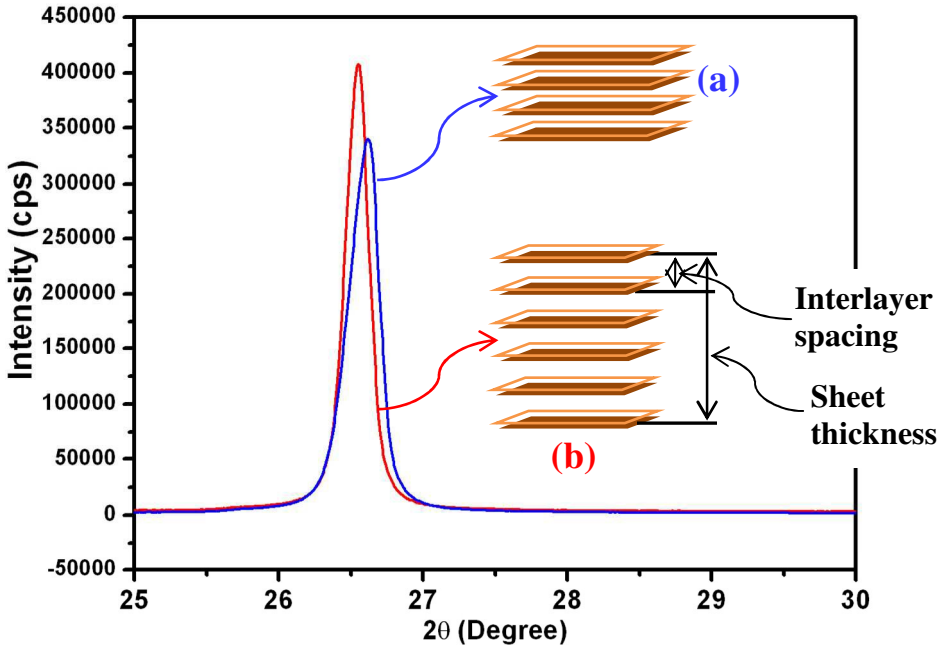


**Fig. 1.** XRD of (a) PEG-Gr-$NS_0$ and (b) PEG-Gr-$NS_3$ samples

Though the interlayer spacing increases, the crystallinity improves in PEG-Gr-$NS_3$ sample. The γ- irradiation induced ordering in graphite was earlier reported by Bin Li *et al.*[25] Well resolved morphology and microstructure of PEG-Gr-$NS_3$ sample is shown in FE-SEM, TEM and HR-TEM images (Fig. 2). Strained curved edge (arrow in FE-SEM) and transparent images of Gr-NS are shown in FE-SEM and TEM images clearly point to the fact that graphite sheet is composed of several layers. HR-TEM images reveals bunch of Gr-NS indicated in region (a) of Fig. 2b. It is observed that, lateral dimension of the graphite is significantly larger than the thickness of the graphite sheet and this is clearly revealed in low resolution TEM and FE-SEM images (Fig. 2a). The lattice fringes show interlayer distance of 0.41 nm corresponds to graphite (002) plane and this is well in agreement with XRD data. In HOPG, the interlayer distance is 0.32 nm.[26] Region (b) in Fig. 2b show localized flaking of few layers of graphene sheets. Regions (c) and (d), typically represents amorphous carbon structure. From this analysis, it is confirmed that distance

of (002) graphite planes are increased due to intercalation of PEG200. It is understood that structure is dominated by a combination of Gr-NS, localized graphene and amorphous carbon constituent.

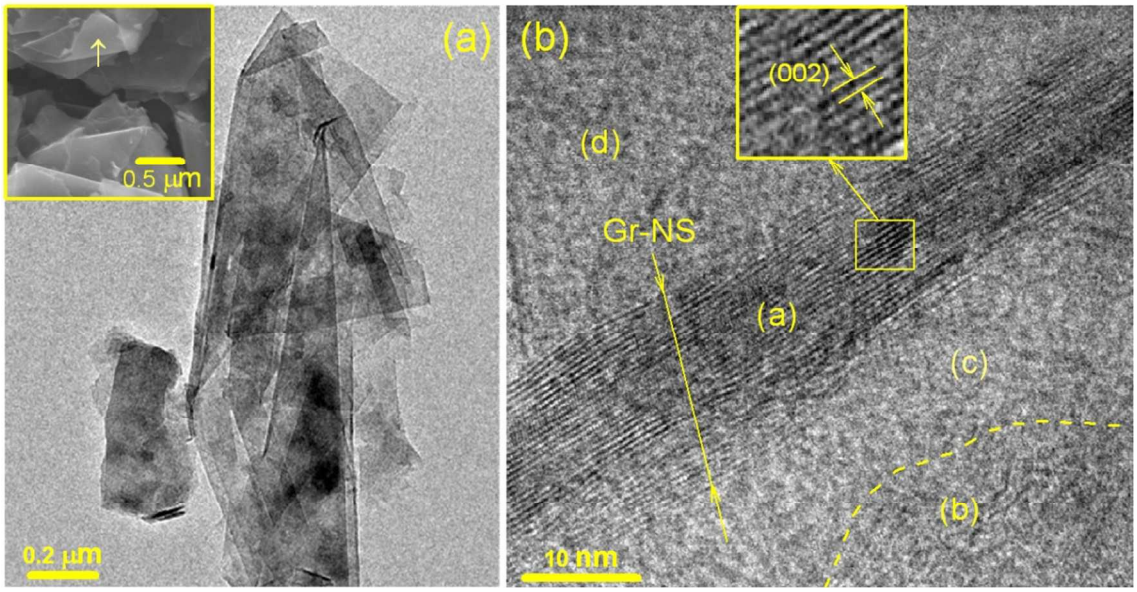


**Fig. 2.** Low resolution (a) and high resolution TEM (b) of PEG-Gr-$NS_3$ sample. Inset in figure 2a shows FE-SEM image of the PEG-Gr-$NS_3$ sample

### 3.2 FTIR analysis

FTIR analysis was conducted to characterize the changes in chemical bonds that occurred during the γ-radiolysis of PEG-Gr-NS. For this analysis, three samples were selected. Figure 3 shows the FTIR spectra of PEG200, PEG-Gr-$NS_0$ and PEG-Gr-$NS_3$ samples. The PEG200 spectrum shows characteristic bands of specific functional groups. The doublet at 2938 and 2872 $cm^{-1}$ belongs to symmetric and antisymmetric $–CH_2$ peaks of alkyl chains, respectively. The peak at 1062 $cm^{-1}$ is assigned to the –C–O–C group.[27] These two characteristic bands and some other bands are appeared in the PEG-Gr-$NS_3$ spectrum, indicating existence of hydrogen bonding of PEG200 to the Gr-NS.[23] Change in color of the PEG-Gr-$NS_3$ dispersed in the PEG200 medium is

a clear indication of chemical reaction followed by grafting which is shown in the digital image. This image was obtained after a month of sample preparation and it clearly shows excellent stability of PEG-Gr-NS dispersion in the PEG200 lube. Peaks related to $–CH_2$ and –C–O–C groups shifted to higher wavenumber, suggesting the occurrence of stronger coordination between oxygen atoms in the –C–O–C group and PEG-Gr-NS.

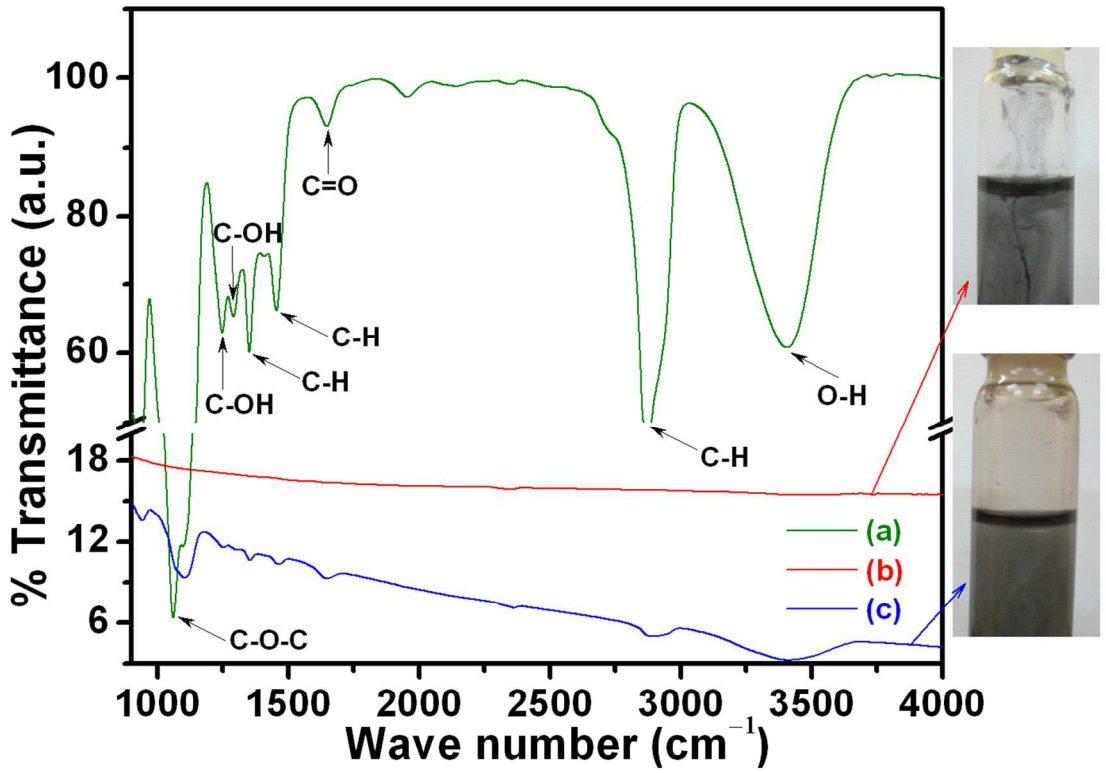


**Fig. 3.** FTIR of (a) PEG200 (b) PEG-Gr-$NS_0$ and (c) PEG-Gr-$NS_3$. Digital images shows change in color due to γ– radiolysis in sample (c) PEG-Gr-$NS_3$

The hydrogen bonding contributes to the shape- stabilization because the PEG200 molecules are tied to the Gr-NS by the confinement effect of strong intermolecular hydrogen bonding which hinder their freedom of motion. The bending vibration of C–OH at 1242 and 1288 $cm^{-1}$ along with C=O stretching vibration at 1651 $cm^{-1}$ originates from hydroxyl (–OH) and carboxyl groups (–COOH) chemically linking with PEG200 and Gr-NS through hydrogen bonding.[22] Carboxylic

acids are polar and it behaves as a hydrogen-bond acceptors (–C=O) and hydrogen-bond donors (–OH) and therefore, participate in hydrogen bonding. Band at 3407 $cm^{-1}$ shows stretching O–H mode of C–OH group in PEG which becomes broader in PEG-Gr-$NS_3$ sample. Absorption at 1342 and 1460 $cm^{-1}$ are attributed to deform vibration of C–H bond existing in PEG200 which conjugates with Gr-NS forming hydrogen bond. From these results, it is confirmed that PEG-Gr-$NS_3$ chemically linking with Gr-NS. However, PEG-Gr-$NS_0$ sample–does not show functional peaks of PEG200 and Gr-NS which clearly indicates the absence of functionlization and chemical grafting. This is visibly reflected in the digital image which shows agglomerated precipitates of Gr-NS.

### 3.3 Raman spectra

Two phonon modes with $E_{2g}$ symmetry at the center of the first Brillouin zone are active in first-order Raman scattering in highly oriented pyrolitic graphite (HOPG), i.e. quasi-perfect infinite ABAB…..stacking of graphene layers. The first one is located at about 43 $cm^{-1}$ and corresponds to anti-phase translational motion of successive layers perpendicular to their normal[28]. It is hardly observable because of its proximity to Rayleigh line. The second one commonly called the G band and it is located at 1580 $cm^{-1}$ corresponds to the zone center vibration of carbon atoms.[29–31] These are the common vibrational characteristics of graphenes and graphite materials. In samples PEG-Gr-$NS_{(0-3)}$ (Fig. 4), the G band appears at 1577–1578 $cm^{-1}$ is close to that of crystalline graphite and it is well in agreement with the XRD data (Fig. 1). In these samples, full width at half maximum (FWHM) of G band is 17.5–18 $cm^{-1}$ which is signature of crystalline structure of graphite.[32,33] Weak feature of D band with $A_{1g}$ symmetry appears at 1345 $cm^{-1}$ as a consequence of a double resonance which involves scattering of the electron by phonon and defect. It is sensitive to the structural changes and attributed to the significant defect

concentration. These defects are mainly in-plane substitutional heteroatoms, vacancies, or grain boundaries/edges.[34] The D* band is bond disordered symmetry and originates from the intra-valley double resonance scattering process.[35] This band involving graphene layers existing at the surface of a graphitic crystal *i.e.* graphene layers which are not sandwiched between two other graphene layers.

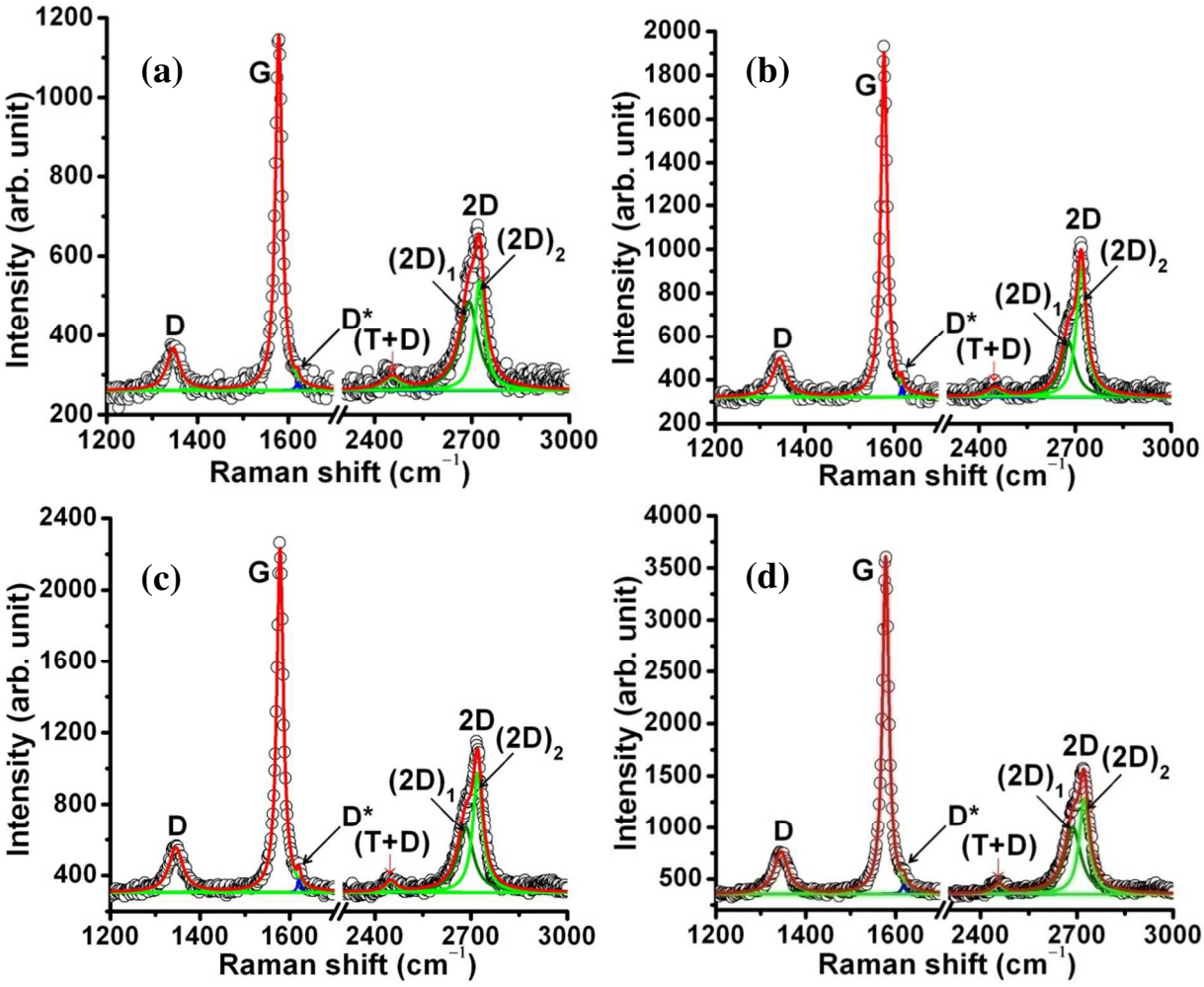


**Fig. 4.** Raman spectra of sample (a) PEG-Gr-$NS_0$ (b) PEG-Gr-$NS_1$ (c) PEG-Gr-$NS_2$ and (d) PEG-Gr-$NS_3$

Integrated intensity ratio I(D)/I(G) is widely used for characterizing the defect concentration in graphite. This ratio is a measure of degree of disorder in the graphite structure and it is inversely proportional to the average size of the $sp^2C$=C cluster.[29,30] Increasing I(D)/I(G) ratio indicates in-plane defects such as interstitials and vacancies and their clusters which eventually result in bond formation, disordering and turbulence of the basal planes. From this analogical point of view, I(D)/I(G) ratio is 0.31 in sample PEG-Gr-$NS_0$ which decreased to 0.21 in sample PEG-Gr-$NS_3$ indicating a reduction in defect concentration (Fig. 5). For both the graphite samples, the Raman spectra exhibits second-order bands and analysis of these bands are equally important to investigate order/disordered state in graphite. In the second-order Raman spectrum, the mode generated at the *K* symmetry point of the Brillouin zone gives rise to the 2D band.[36]

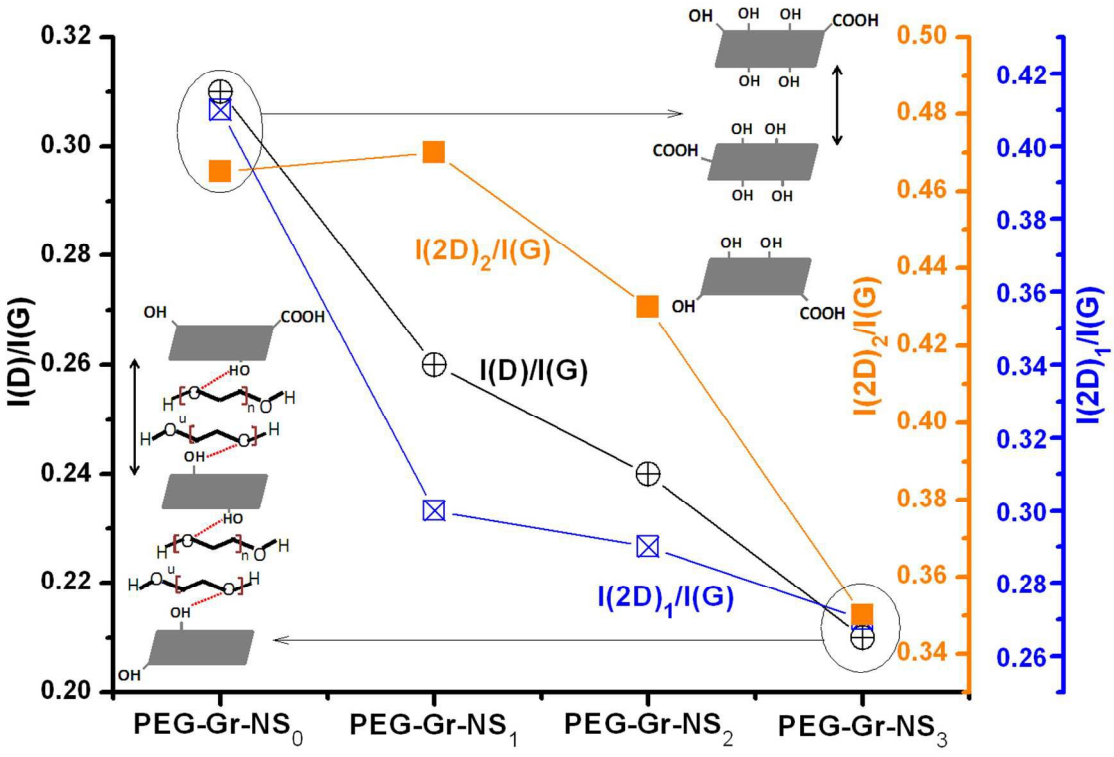


**Fig. 5.** γ- radiolysis of PEG-Gr-NS vs structural changes considering change in I(D)/I(G), $I(2D)_1$/I(G) and $I(2D)_2$/I(G) ratio

This band is active for a HOPG due to two phonons emission having equal and opposite wave-vectors and hence conserve momentum. Since zone-boundary phonons do not satisfy the Raman fundamental selection rule and thereby, it is not observed in the first order Raman spectra of defect-free graphite.[28] Such phonons give rise to a D band Raman peak at 1345 $cm^{-1}$ in defected graphite. The 2D band arises from a splitting in the π-electron dispersion and is attributed to strong interaction between the basal planes of graphite. Results show that 2D band splits into $(2D)_1$ and $(2D)_2$ bands centered at 2682 and 2721 $cm^{-1}$, respectively.[37,38] Splitting of these bands is described as a characteristic feature of 3D graphite lattice.[28,36,39] These bands are associated with contributions from regions near the *K* and *M* points of wave vector, respectively.[40] The $I(2D)_1/I(G)$ and $I(2D)_2/I(G)$ ratios are high in sample PEG-Gr-$NS_0$ which consistently decreases and become smallest in sample PEG-Gr-$NS_3$ signifying less stacking faults in the graphite sheets.[41] The relationship of I(D)/I(G) with $I(2D)_1/I(G)$ and $I(2D)_2/I(G)$ ratios is clearly shown in Fig. 5. The decreases of these ratios describe reduction in above mentioned defects and this is schematically shown in inset (Fig. 5). Interlayer distance due to intercalation of PEG increased and preserving the structural integrity. The defects reduced due to γ-irradiation which induces reduction of oxygen functionalities. This acts to promote chemical grafting of PEG between the graphite sheets. The band at 2450–2453 $cm^{-1}$ can be attributed to the Raman-active first overtone of a Raman-inactive graphitic lattice vibration mode that occurs at 1220 $cm^{-1}$.[38,42]

### 3.4 HR-XPS analysis

To reveal the carbon-oxygen groups and chemical structure, XPS C 1s and O 1s spectra were obtained. The spectra were fitted by the Gaussian-Lorentzian function to respective components with the characteristic binding energy (BE) values for C 1s and O 1s photoelectrons characteristic for the particular groups. Figure 6 shows high resolution C 1s and O 1s XPS

spectra of PEG-Gr-$NS_0$ and PEG-Gr-$NS_3$ samples. The doublet peak of C 1s spectrum can be deconvoluted into three chemically shifted distinct components C-C $sp^2$, C=C $sp^3$ and C-OH/C-O-C at BE 284.27, 285.26 and 286.65 eV, respectively, in PEG-Gr-$NS_0$ (Fig. 6$a_i$).[43,44]

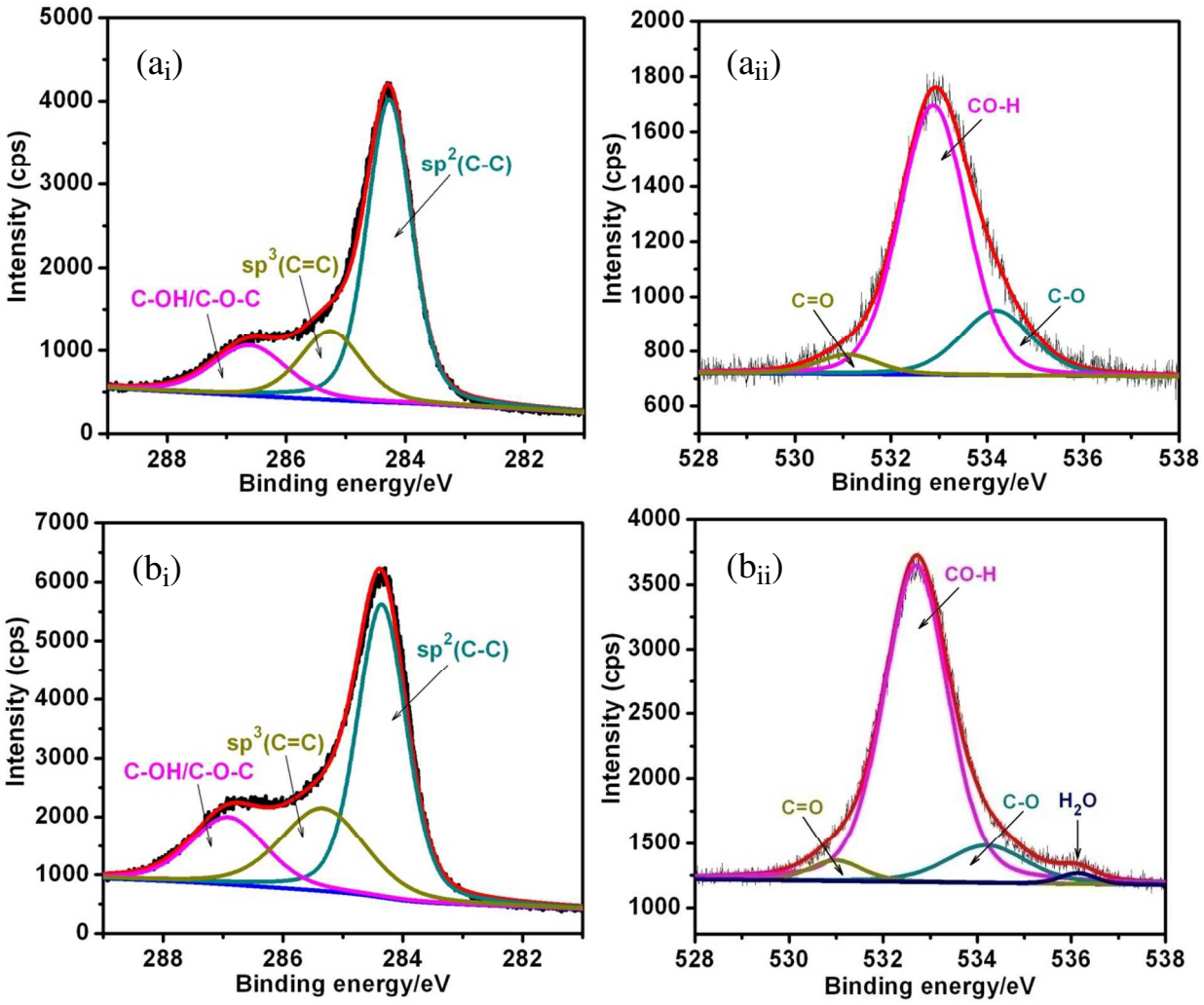


**Fig. 6.** XPS of C 1s ($a_i$) and O 1s ($a_{ii}$) of PEG-Gr-$NS_0$ and C 1s ($b_i$) and O 1s ($b_{ii}$) of PEG-Gr-$NS_3$

These peaks are slightly shifted to 284.3, 285.3 and 286.9 eV in sample PEG-Gr-$NS_3$ (Fig. 6$b_i$). Consequently, in this sample, a broad O 1s peak is deconvoluted into three different chemically shifted components with major hydroxyl/epoxy groups C-OH/C-O-C at 532.8 eV. The other two peak pertain to carboxyl C-O and carbonyl C=O functionality existing at 534.1 and 531.1 eV,

respectively (Fig. 6a$_{ii}$). However, in PEG-Gr-NS$_3$, a broad O 1s peak is deconvoluted into four chemically shifted components with additional minor peak of chemisorbed $H_2O$ at 536.13 eV (Fig. 6b$_{ii}$). Such a wide range of BE is attributed due to the presence of water in PEG200 incorporated Gr-NS. The carbon functional groups create hydrogen bonds with water molecules via oxygen and/or hydrogen.[45,46] High content of C-C $sp^3$ in PEG-Gr-NS$_3$ is explained by the presence of extensively functionalized oxygen and possible linking of alkyl groups to carbon atoms. The C-OH hydroxyl group from O 1s is placed at higher BE compared to C-OH/C-O-C group bonded to carbon. This is observed in C 1s spectra and indicates presence of water molecules attached to functionalized oxygen and incorporated between the Gr-NS. This is also evident from the FTIR analysis. In both the samples, oxygen groups resulting from O 1s spectra is approximately similar to the respective components resulting from fitting of C 1s spectra. It is noticed that CO-H component in O 1s increases with increase in CO-H/C-O-C component in C 1s spectra in PEG-Gr-NS$_3$. In these samples, presence of carbonyl group indicating C=O interaction with the adsorbed water via hydrogen bonding. The C=C $sp^2$/C-C $sp^3$ ratio is 3.3 and 2.6 in PEG-Gr-NS$_0$ and PEG-Gr-NS$_3$ samples, respectively. Therefore, C=C $sp^2$/[C-OH/C-O-C] and C-C $sp^3$/[C-OH/C-O-C] are 3.81 and 2.78 in PEG-Gr-NS$_0$. These values decreased to 1.15 and 1.08 in PEG-Gr-NS$_3$ sample which is a clear indication of increased PEG200 functionlization and improved graftification. The O 1s intensity ratio of oxygen functional groups with respect to the C-C $sp^3$ and C=C $sp^2$ domains increase in PEG-Gr-NS$_3$ lead to the formation of the epoxide (C-O-C) linkage which results in the increased interlayer spacing.[47]

### 3.5 Friction and lubrication mechanism of hybrid PEG-Gr-NS dispersed PEG200

Friction coefficient of PEG200 and PEG-Gr-NS$_0$ is having similar magnitude ~0.15 (Fig. 7). This indicates that without γ- irradiation PEG-Gr-NS does not have friction reducing capability

due to absence of chemical grafting with PEG200. However, this value is consistently decreased with increase in γ-irradiation dose and becomes lowest ~0.09 in PEG-Gr-$NS_3$ (curve (e)) sample and the average value is plotted in inset of Fig. 7.

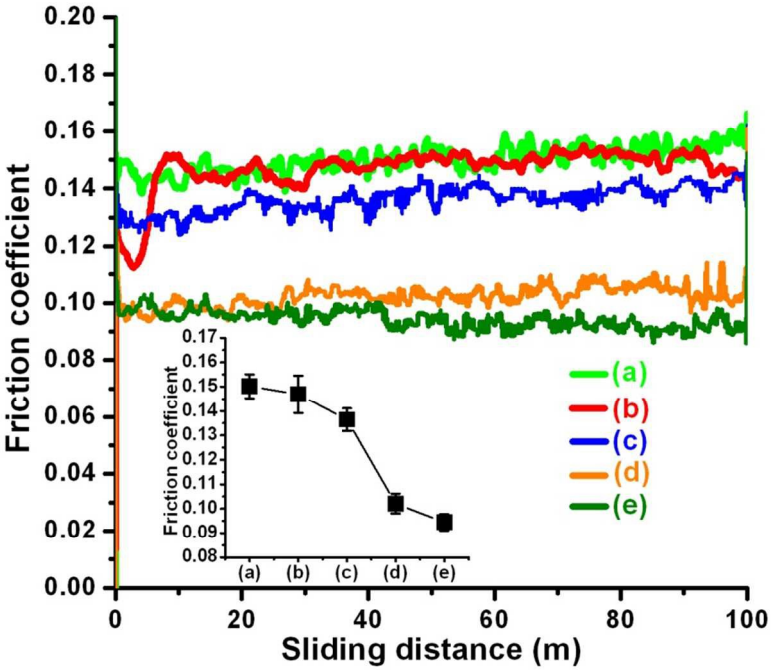


**Fig. 7.** Friction coefficient of sample (a) PEG200 (b) PEG-Gr-$NS_0$ (c) PEG-Gr-$NS_1$ (d) PEG-Gr-$NS_2$ and (e) PEG-Gr-$NS_3$. Inset shows average value of friction coefficient with deviation. Tribo-test condition: PEG-Gr-NS concentration 0.03 mg $mL^{-1}$, load 1 N, sliding speed 3 cm/s.

Friction coefficient value of PEG-Gr-$NS_2$ and PEG-Gr-$NS_3$ are approximately close (Fig. 7d-e) which indicates that effect of irradiation becomes ineffective after certain critical dose. In the next step, the concentration of PEG-Gr-$NS_3$ was varied in PEG medium to obtain the lowest value of friction coefficient (Fig. 8). This value was lowest ~0.09 in concentration of 0.03 mg $mL^{-1}$ and this is clearly shown in the inset of Fig. 8. At the lowest concentration 0.02 mg $mL^{-1}$, this value is slightly higher as compared to 0.03 mg $mL^{-1}$ and consistently increases with increase in concentration. This indicates the sensitivity of friction to concentration of PEG-Gr-NS in lube medium. At higher concentration, it is assumed that Gr-NS collide in contact which

may generate wear and disrupt the lamellar motion.[48] In contrast, effective lubrication process decreases when the concentration of PEG-Gr-NS is small enough which does not properly fill the contact interfaces during the sliding. From here, three tribo-test conditions such as only PEG200, PEG-Gr-$NS_0$ and PEG-Gr-$NS_3$ were selected for investigating the lubrication mechanism. Purpose to choose the above mentioned condition is meaningful in order to understand lubrication mechanism when only PEG200 was introduced during the tribo-test. Consequently, comparison of lubrication in other two conditions where PEG-Gr-$NS_0$ belongs to non-irradiated sample showing highest value of friction coefficient and PEG-Gr-$NS_3$ displayed lowest one. Other two samples PEG-Gr-$NS_1$ and PEG-Gr-$NS_2$ shows close friction results with PEG-Gr-$NS_0$ and PEG-Gr-$NS_3$, respectively.

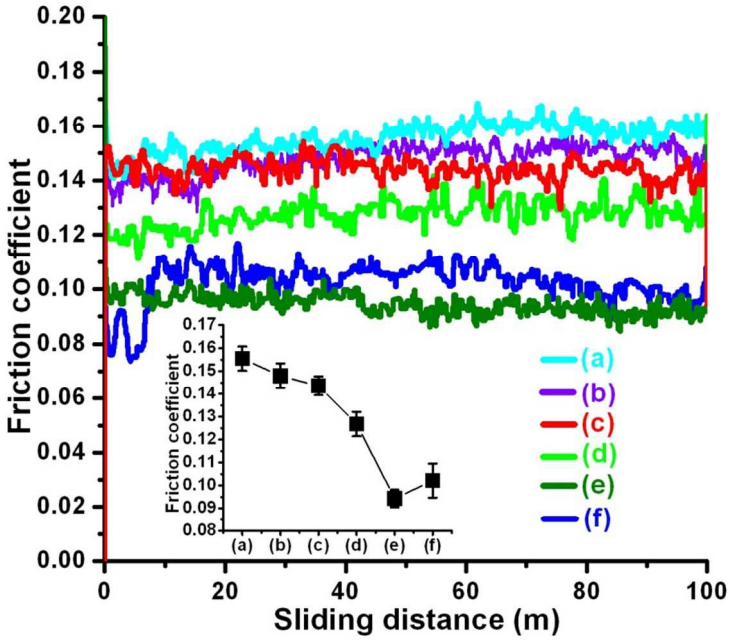


**Fig. 8.** Friction coefficient of PEG-Gr-$NS_3$ sample with change in concentration (a) 0.3 (b) 0.2 (c) 0.1 (d) 0.05 (e) 0.03 (f) 0.02 mg $mL^{-1}$. Inset shows average value of friction coefficient with deviation. Tribo-test condition: Load 1 N, sliding speed 3 cm/s.

It is clearly seen that wear width is approximately similar in PEG200 and PEG-Gr-$NS_0$ (Fig. 9a-b) and it is greatly reduced in PEG-Gr-$NS_3$ tribo-condition (Fig. 9c). Magnified image of wear track in PEG200 lubricated condition shows deep scratches, cracks, grooves and delaminated deformed ripples, suggesting the severe plastic deformation along with adhesive wear. However, wear track is smoother in the PEG-Gr-$NS_3$ lubricated condition. Penetration depth is also greatly reduced in PEG-Gr-$NS_3$ sample (Fig. 10).

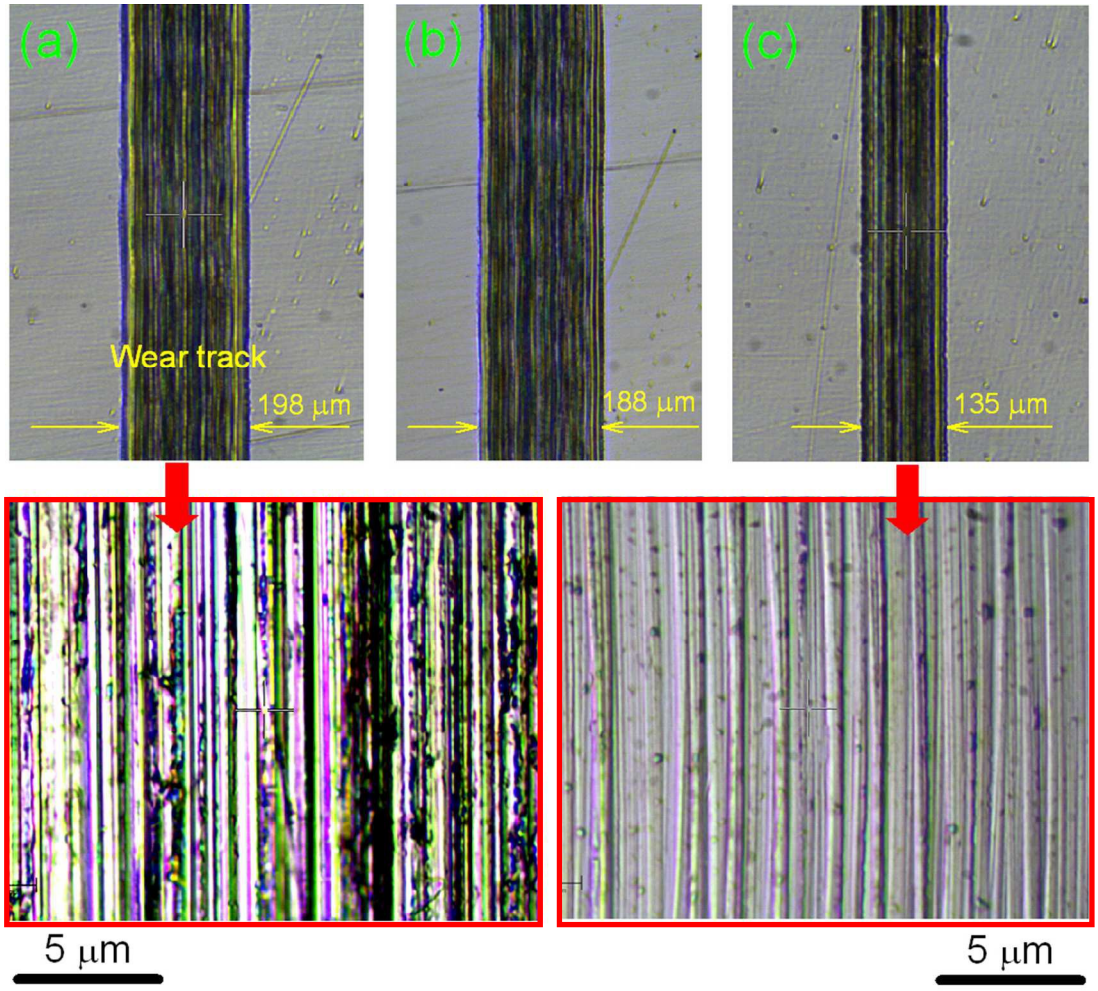


**Fig. 9.** Optical image of wear track and ball scar of (a) PEG200 (b) PEG-Gr-$NS_0$ and PEG-Gr-$NS_3$ tribo-test condition.

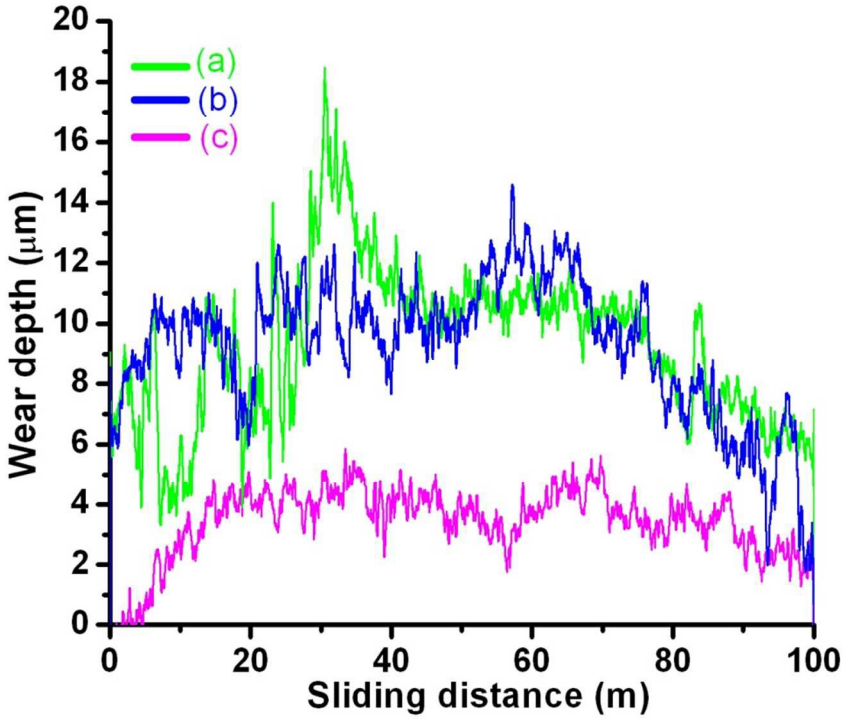


**Fig. 10.** In-situ penetration depth in steel disc of (a) PEG200 (b) PEG-Gr-$NS_0$ and PEG-Gr-$NS_3$ tribo-test condition

Other two samples PEG200 and PEG-Gr-$NS_0$ show high penetration depth and the curves are unstable with large periodic deviation which is signature of high periodic wear and formation of scratches and grooves. This indicates that the work done in friction is directly proportional to the wear of the contacting bodies. Such relationship is important to investigate from chemical point of view. For the analysis, after the tribology test, the buried lubricant from the contacting bodies was collected for FTIR studies. Ratio of –C–H/O–H is greatly reduced and this is related to the oxidation of decomposed methyl group which chemically interact with atmospheric moisture resulting highly disordered oxygenious Gr-NS (Fig. 11). This reaction enhances formation of carbonyl and carboxyl functional groups along with a new peak related to carbonyl C=O stretching mode appearing at 1736 $cm^{-1}$. Results confirm the existence of hydroxyl and carbonyl

groups in the PEG-Gr-$NS_0$ and PEG-Gr-$NS_3$ systems which are in agreement with the proposed structural models.[16]

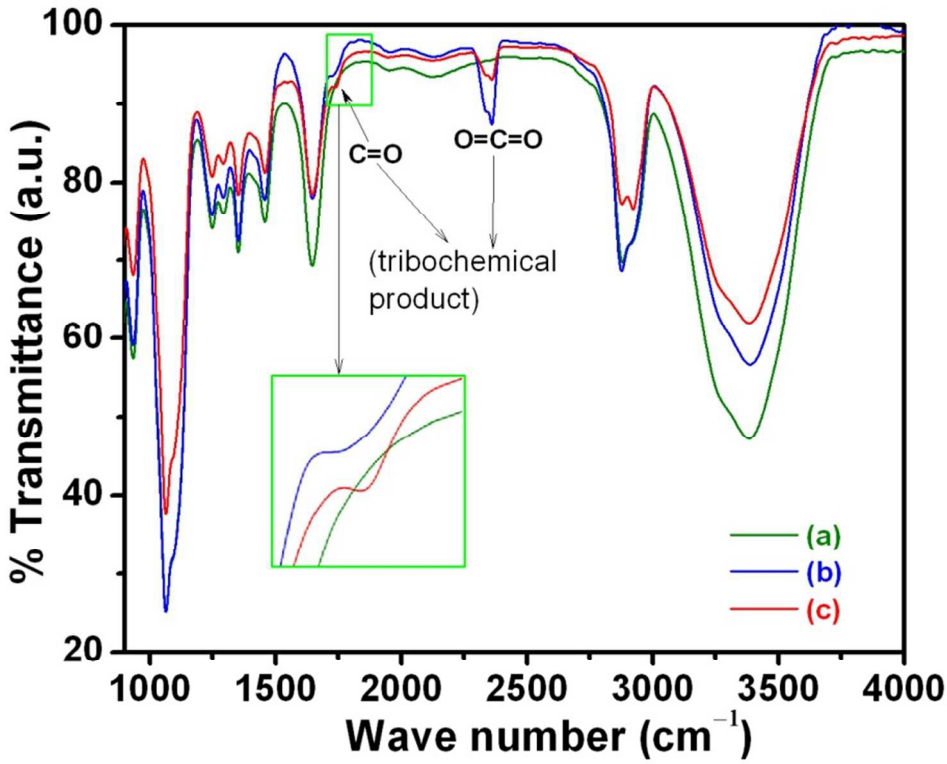


**Fig. 11.** FTIR of buried lubricant collected from the tribo-contact after the test (a) PEG200 (b) PEG-Gr-$NS_0$ and (c) PEG-Gr-$NS_3$

This indicates that the main functional groups in PEG200 and Gr-NS are preserved after the tribology test. In addition, the FTIR results suggest that there are C=O and O–H groups in both PEG and Gr-NS, which indicates possible hydrogen bonding between PEG and Gr-NS. Antisymmetric stretching mode at 2342 cm$^{-1}$ belongs to tribochemical product of $CO_2$ molecules entrapped in Gr-$NS_0$ and Gr-$NS_3$ samples which is a consequence of oxidation of carbon. The shift in peak position and change in relative intensity attributes grafting through hydrogen bonding. However, functionalization in buried tribo-tested PEG200 sample remains same as compared to pure PEG200, indicating absence of weak/strong chemical interactions. The

similarities in tribo-functional changes in PEG-Gr-$NS_0$ and PEG-Gr-$NS_3$ do not satisfactorily answer the large difference in friction coefficient. This may be related to small amount of PEG-Gr-NS dispersed in lube medium of PEG200. Therefore, Raman spectra inside the wear tracks of above mentioned tribo-conditions are carried out to investigate formation of adsorbed tribo-film. Very weak feature of carbonaceous material was detected around 1320–1460 $cm^{-1}$ inside the wear track (Fig. 12a). This is a product of tribochemical reaction of PEG200 with steel surface. Such carbonaceous material is formed due to the presence of small amount of carbon in steel and decomposed hydrocarbon of PEG200 which is adsorbed product of the wear track. This behavior is observed when only PEG200 is introduced in tribo-contact. However, strong feature of Raman peaks inside the wear track reveals signature of graphite/a-C in PEG-Gr-$NS_0$ sample (Fig. 12b). In this case, the I(D)/I(G) ratio increases to 1.26 which clearly signifies large quantity of in-plane defects such as heteroatoms, grain boundaries and formation of aliphatic chains. These results points to structural instability associated with basal planes. The D* band (1616 $cm^{-1}$) becomes stronger with the newly appeared (D+G) line (2940 $cm^{-1}$) is a signature of defects and characteristics of these defects are mentioned above in detail (section 3.3). The G band intensity does not changed much but it becomes broad because of the appearance of shoulder D* line contributing to increase in intensity of D band. Increase in I(D)/I(G) and I(D*)/I(G) ratios clearly induce increase in C=C $sp^2$ boundaries and heteroatoms.[49] The shift in G band and increase in D band FWHM are associated with the formation of more amount of C-C $sp^3$ carbon atoms in the graphite lattice. This indicates oxidation of Gr-NS which tends to distort in-plane C=C $sp^2$ domains.[30] In addition, increases in $I(2D)_1/I(G)$ and decreases in $I(2D)_2/I(G)$ ratios to 0.5 and 0.2, respectively, indicate enhanced stacking defects in graphite. An additional higher-order band is

observed at 2942cm$^{-1}$, which is a combination of G and D (G+D) mode, characteristic of a disordered graphitic structures.[50]

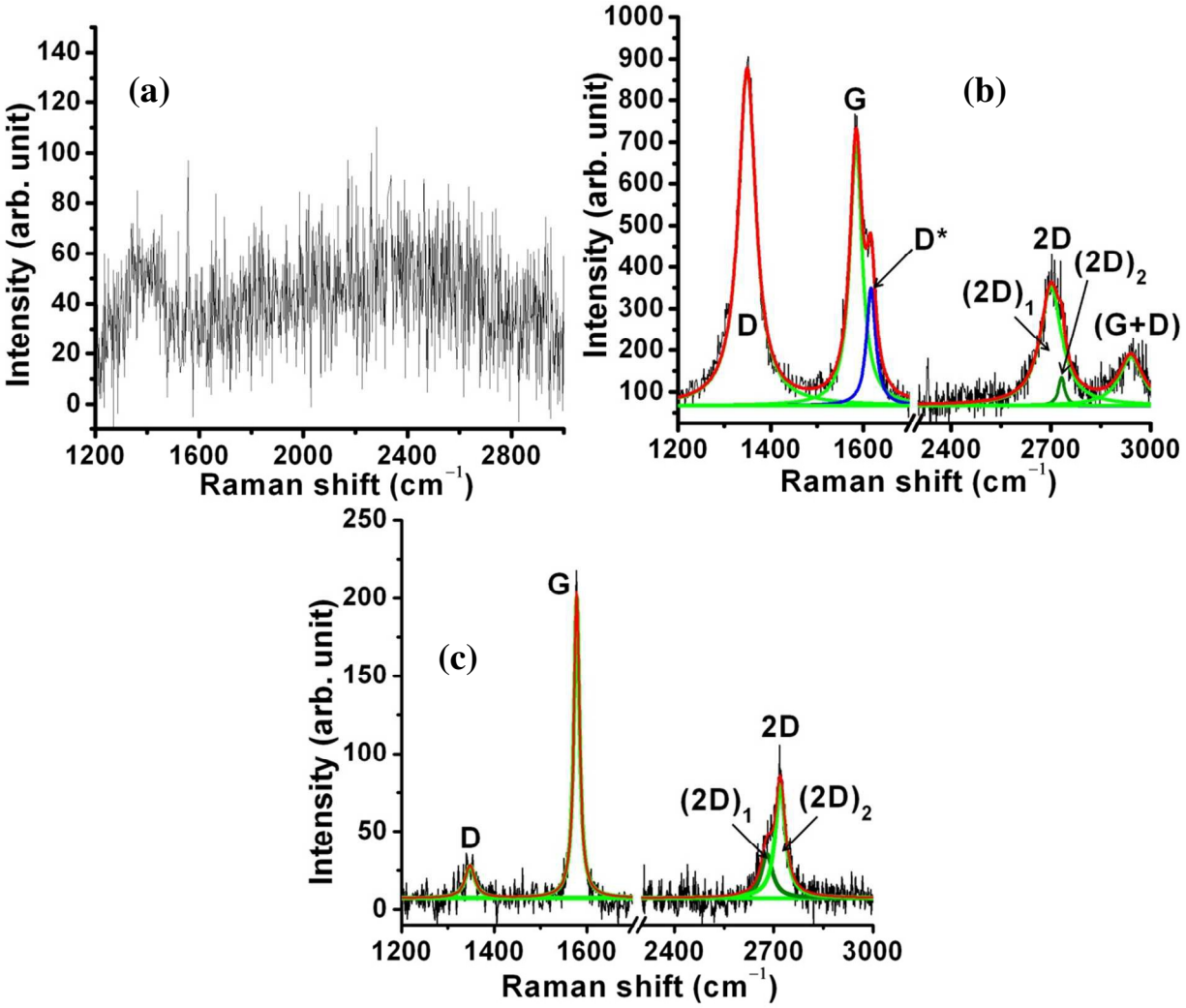


**Fig. 12.** Raman spectra inside the wear track of steel sample (a) PEG200 (b) PEG-Gr-NS$_0$ and (c) PEG-Gr-NS$_3$.

Above mentioned Raman characteristics indicate that defects in Gr-NS are greatly contributed by oxidation[41] which is related to dissipation of high frictional energy. Absence of PEG200 functionlization in PEG-Gr-NS$_0$ samples is the reason behind high frictional energy which causes

to produce oxidation and structural disorder in Gr-NS. Although, a tribolayer is formed in the steel wear track, the friction does not reduce due to oxidized graphite structure. However, Raman spectral characteristic such as shape and peak position inside the wear track lubricated with PEG-Gr-$NS_3$ are similar to virgin γ-irradiated PEG-Gr-$NS_3$ sample. The comparison can be seen in Fig. 4d and Fig. 12c. The I(D)/I(G) ratio decreased to 0.13 which indicates reduction of various in-plane defects. This in-tern induces ordering in the basal plane. Ratio of $I(2D)_1/I(G)$ and $I(2D)_2/I(G)$ is 0.17 and 0.4, respectively, which signifies reduction in c-axis stacking defects.[41] Absence of D* and (G+D) bands including the above mentioned spectral characteristics indicates ordering in graphite lattice. This shows that the structural stability of Gr-NS which is mediated through the chemical interaction with functional groups of PEG200 and functionalized Gr-NS. Linkage of the PEG200 and Gr-NS through hydrogen bonding acts as a molecular spring in normal direction which counters the tribo-induced contact stress. This is schematically represented in Fig. 13. Specifically, this mechanism, absorb the energy produced in normal direction through molecular bridging, helping to reduce the deformation and wear. This effect is possible when O–H---O bond length integrated between Gr-NS-PEG changes due to change in electrostatic potential. Consequently, interlayer graphite sheets easily shear when distance between the sheets increases due to intercalation of PEG200 molecules. Effective interlayer shearing reduces energy in lateral direction, hence tangential force decreases. The hydrogen bonding between PEG200 and Gr-NS contributes to the shape- stabilizer. This happens when PEG molecules are tied to the surface of Gr-NS by the confinement effect of strong intermolecular hydrogen bonding aligned parallel to the graphite sheet.[51] The graphite tribolayer is possibly formed when cohesive interaction between the sliding surfaces and the PEG200 is locally disrupted by the critical contact pressure and cleavage of hydrogen bonding due to the

shear force. In this condition, the small domain of graphite tribolayer is deposited on the steel wear track.[52] This layer is sustainable and preserved due to dissipation of less frictional energy. The remarkable lubricating effect exists even in case of tribo-film of nanometer scale.[52,53] This is an indication of a predominant surface rather than a bulk effect. In macroscale studies, sliding over the various nano-objects reduced friction and wear due to the multiple nano-object contacting interfaces.[54] The lowest friction coefficient and wear in macroscale contact occur with nanoparticles due to the reduced contact area.

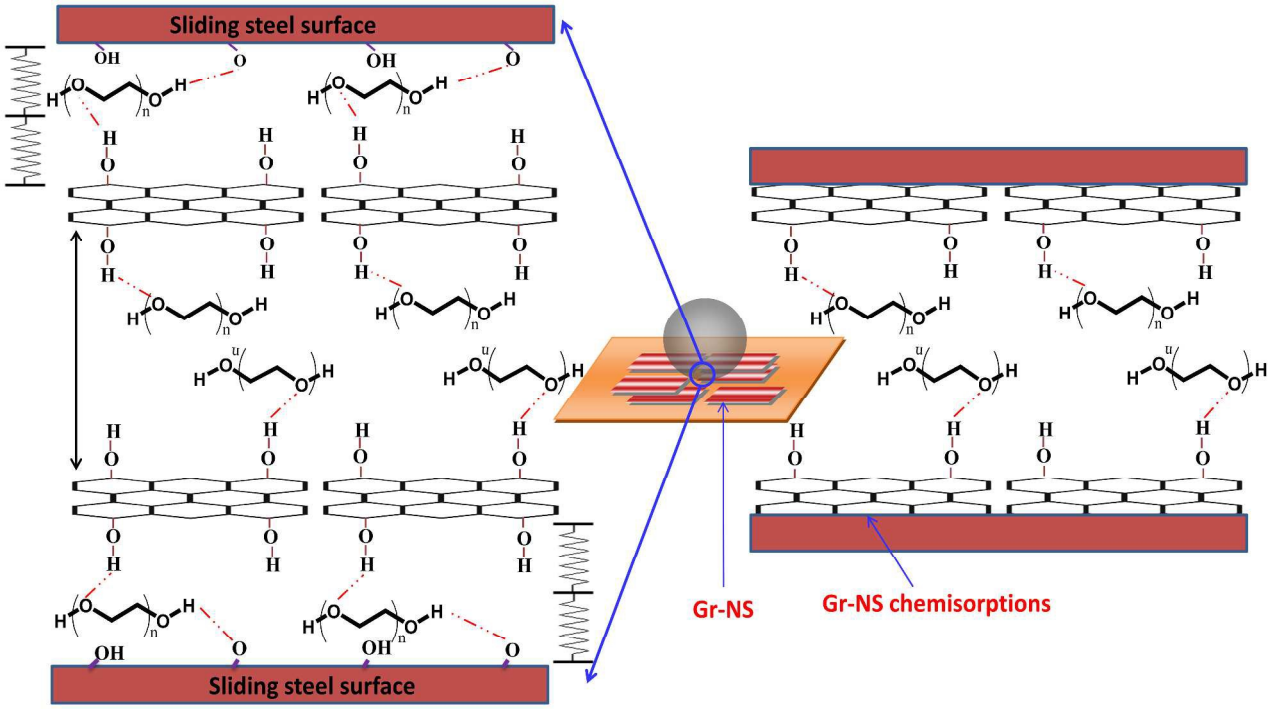


**Fig. 13.** Tribo-contact condition and lubrication mechanism of PEG-Gr-NS dispersed in poly(ethylene glycol)

## 4 Conclusion

The γ-irradiation process reduces oxygen functionalities of Gr-NS in the presence of PEG200, resulting ordered structure of graphite nanosheets. Hydroxyl functional group of PEG200 is

chemically grafted with hydroxyl, carbonyl and carboxylic groups of Gr-NS through hydrogen bonding. This is possible due to the production of active radicals through the solvent γ-radiolysis which enhances the dispersion capability of Gr-NS in PEG200 lube medium. Though the oxygen functionality reduces, the inter-planer distance of Gr-NS is increased due to intercalation of PEG200 molecules, preserving the structure orderly. Tribological properties of PEG200 grafted Gr-NS with the minute concentration of 0.03 mg $mL^{-1}$ in PEG200 lubricated condition showed significant reduction in friction coefficient and wear. This value was 0.15 in PEG200 lubricated medium and reduced to 0.09 in hybrid PEG-Gr-NS with PEG200 lubricated condition. Wear loss from the steel disc was also reduced up to 32%. Such an improvement in tribological properties are explained by the (a) effective shearing of graphite interlayer due to grafting of PEG200 with Gr-NS (b) attachment of PEG-Gr-NS functionalize group with sliding surfaces (c) formation of chemisorbed Gr-NS tribo-film in wear track. The deposited Gr-NS prevent the direct contact between the tribo-pairs and exhibited remarkable improvement in wear property.

## References

1 K. Holmberg, P. Andersson and A. Erdemir, *Tribol. Int.*, 2012, 47, 221–234.

2 J. Cumings, A. Zettl, *Science* 2000, 289, 602–604.

3 M. R. Falvo, R. M. Taylor, A. Helser, V. Chi, Jr. F. P. Brooks, S. Washburn and R. Superfine, *Nature* 1999, 397, 236–238.

4 R. Luthi, E. Meyer, H. Haefke, L. Howald, W. Gutmannsbauer and H. J. Guntherodt, *Science* 1994, 266, 1979–1981.

5 M. Dienwiebel, G. S. Verhoeven, N. Pradeep and J. W. M. Frenken, *Phys. Rev. Lett.*, 2004, 92, 126101–126104.

6 D. Berman, A. Erdemir and A. V. Sumant, *Mater. Today* 2014, 17, 31–42.

7 C. M. Mate, G. M. McClelland, R. Erlandsson and S. Chiang, *Phys. Rev. Lett.*, 1987, 59, 1942–1945.

8 L. Rapoport, N. Fleischer and R. Tenne, *Adv. Mater.*, 2003, 15, 651–655.

9 C. Dae-Hyun, L. Wang, K. Jin-Seon, L. Gwan-Hyoung, K. Eok Su, L. Sunhee, L. S. Yoon, J. Hone and L. Changgu, *Nanoscale*, 2013, 5, 3063–3069

10 P. Jibin, W. Shanhong, Z. Wenjie, M. Yufei, Z. Xiaoqian, W. Liping and X. Qunji, *J. Phys. Chem.*, C 2011, 115, 13275–13284

11 K. Sangita, O. P. Sharma, G. Rashi, H. P. Mungse, K. Aruna, N. Kumar, H. Sugimura and O. P. Khatri, *ACS Appl. Mater. Interf.*, 2015, 7, 3708–3716.

12 H. P. Mungse and O. P. Khatri, *J. Phys. Chem. C* 2014, 118, 14394–14402.

13 X. Feng, S. Kwon, J. Y. Park and M. Salmeron, *ACS Nano* 2013, 7, 1718–1724.

14 K. Varsha, P. Minh-Quan, K. Nitee, Y. Hae-Sung, K. Chung-Soo, P. A. Jae-IL and Sung-Hoon, *ACS Appl. Mater. Interf.*, 2013, 5, 4063-4075.

15 H. Liang, Y. Bu, J. Zhang, Z. Cao and A. Liang, *ACS Appl. Mater. Interf.*, 2013, 5, 6369–6375.

16 D. R. Dreyer, S. Park, C. W. Bielawski and R. S. Ruoff, *Chem. Soc. Rev.*, 2010, 39, 228–240.

17 R. D. Arnell and D. G. Teer, *Nature* 1968, 218, 1155–1156.

18 X. Jinkun, Z. Lei, Z. Kechao, L. Jianguo, X. Xinlin and L. Zhiyou, *Carbon* 2013, 65, 53–62.

19 J. C. Rietsch, P. Brender, J. Dentzer, R. Gadiou, L. Vidal and C. Vix-Guterl, *Carbon* 2013, 55, 90–97.

20. J. A. Ruan and B. Bhushan, *J. Appl. Phys.*, 1994, 76, 8117–8120.

21 L. Ze, Y. Jiarui, G. Francois, Z. L. Jefferson, L. Yilun, W. Yibing, Y. Yanlian, C. Yao and Z. Quanshui, *Phys. Rev.Lett.*, 2012, 108, 205503–205507.

22 S. Zhang, Q. Tao, Z. Wang and Z. Zhang, *J. Mater. Chem.*, 2012, 22, 20166–20169.

23 C. Wang, L. Feng, H. Yang, G. Xin, W. Li, J. Zheng, W. Tian and X. Li, *Phys. Chem. Chem. Phys.*, 2012, 14, 13233–13238.

24 Y. W. Zhang, H. L. Ma, Q. L. Zhang, J. Peng, J. Q. Li, M. L. Zhai and Z. Z. Yu, *J. Mater. Chem.*, 2012, 22, 13064–13069.

25 L. Bin, Y. Feng, K. Ding, G. Qian, X. Zhang and J. Zhang, *Carbon* 2013, 60, 186 –192.

26 J. Hwang, J. P. Carbotte, S. Tongay, A. F. Hebard and D. B. Tanner, *Phys. Rev. B* 2011, 84, 41410–41413.

27 G. Mani, S. M. J. Yousuf, V. Elangovan and S. Balasubramanian, *J. Mater. Chem.*, B 2014, 2, 418–427.

28 R. J. Nemanich and S. A. Solin, *Phys. Rev. B* 1979, 20, 392–401.

29 A. C. Ferrari and J. Robertson, *Phys. Rev. B* 2001, 64, 75414–75427.

30 A. C. Ferrari and J. Robertson, *Phys. Rev. B* 2000, 61, 14095–14107.

31 A. C. Ferrari and D. M. Basko, *Nature Nanotechnol.* 2013, 8, 235–246.

32 C. Beny-Bassez and J. N. Rouzaud, *Scanning Electron Microscopy* 1985, 1, 119-132.

33 O. Beyssac, J. N. Rouzaud, B. Goffe, F. Brunet and C. Chopin, *Contrib. Mineral. Petrol.* 2002, 143, 19–31.

34 L. M. Malard, M. A. Pimenta, G. Dresselhaus and M. S. Dresselhaus, *Phys. Report* 2009, 473, 51–87.

35 L. Nikiel and P. W. Jagodzinski, *Carbon* 1993, 31, 1313–1317.

36 M. A. Pimenta, G. Dresselhaus, M. S. Dresselhaus, L. G. Cancado, A. Jorio and R. Saito, *Phys. Chem. Chem. Phys.*, 2007, 9, 1276–1290.

37 E. del Corro, A. O. de la Roza, M. Taravillo and V. G. Baonza, Carbon 2012, 50, 4600–4606.

38 P. H. Tan, Y. M. Deng and Q. Zhao, *Phys. Rev. B* 1998, 58, 5435–5439.

39 L. G. Cancado, K. Takai, T. Enoki, M. Endo, Y. A. Kim, H. Mizusaki, N. L. Speziali, A. Jorio and M. A. Pimenta, *Carbon* 2008, 46, 272 –275.

40 A. C. Ferrari, J. C. Meyer, V. Scardaci, C. Casiraghi, M. Lazzeri, F. Mauri, S. Piscanec, D. Jiang, K. S. Novoselov, S. Roth and A. K. Geim, *Phys. Rev. Lett.*, 2006, 187, 187401–187404.

41 K. Karthikeyan, V. Murugan, Y. Kyusik and S. J. Kim, *Carbon* 2013, 53, 38–49.

42 A. Sadezky, H. Muckenhuber, H. Grothe, R. Niessner and U. Poschl, *Carbon* 2005, 43, 1731–1742.

43 L. Stobinskia, B. Lesiaka, A. Malolepszy, M. Mazurkiewicz, B. Mierzwa, J. Zemek, P. Jiricek and I. Bieloshapk, *J. Electron. Spectrosc. Relat. Phenom.*, 2014, 195, 145–154.

44 B. Lesiak, L. Stobinski, A. Malolepszy, M. Mazurkiewicz, L. Kövér and J. Tóth, *J. Electron. Spectrosc. Relat. Phenom.*, 2014, 193, 92–99.

45 A. Buchsteiner, A. Lerf and J. Pieper, *Phys. Chem. B* 2006, 110, 22328–22338.

46 M. Acik, C. Mattevi, C. Gong, G. Lee, K. Cho, M. Chhowalla and Y. J. Chabal, *ACS Nano* 2010, 4, 5861–5868.

47 D. W. Lee and J. W. Seo, *J. Phys. Chem.*, C 2011, 115, 2705–2712.

48 O. Elomaa, V. K. Singh, I. A. Iyer, T. J. Hakala and J. Koskinen, *Diamond Relat. Mater.*, 2015, 52, 43–48.

49 Z. Zafar, Z. H. Ni, X. Wu, Z. X. Shi, H. Y. Nan, J. Bai and L. T. Sun, *Carbon* 2013, 61, 57–62.

50 Y. Wang, D. C. Alsmeyer and R. L. McCreery, *Chem. Mater.*, 1990, 2, 557–563.

51 Q. Guo-Qiang, L. Cheng-Lu, B. Rui-Ying, L. Zheng-Ying, Y. Wei, X. Bang-Hu and Y. Ming-Bo, *Sol. Energ. Mat. Sol. Cells* 2014, 123, 171–177.

52 H.P. Mungse, N. Kumar and O.P. Khatri, *RSC Adv* 2015, 5, 25565–25571.

53 T. Huang, T. Li, Y. Xin, B. Jin, Z. Chen, C. Su, H. Chena and S. Nutt, *RSC Adv.* 2014, 4, 19814–19823.

54 D. Maharaj and B. Bhushan, *Nanoscale*, 2014, 6, 5838–5852.

AUTHOR INFORMATION

**Corresponding Author**

*Email: niranjan@igcar.gov.in, phystribology@gmail.com

Tel.: +91 44 27480500 (ext. 22537)

Fax: +914427480081

**Notes**

The authors declare that there is no competing financial interest

ACKNOWLEDGMENT

B. Gupta would like to acknowledge DST, New Delhi for Inspire Fellowship award. The contribution of Shailesh Joshi (IGCAR) for FTIR and IITM Chennai is acknowledges for HR-TEM characterizations, respectively. We thank M. P. Janwadker, Director, MSG and Dr. P.R. Vasudev Rao, Director, IGCAR for support.

## Graphical abstract

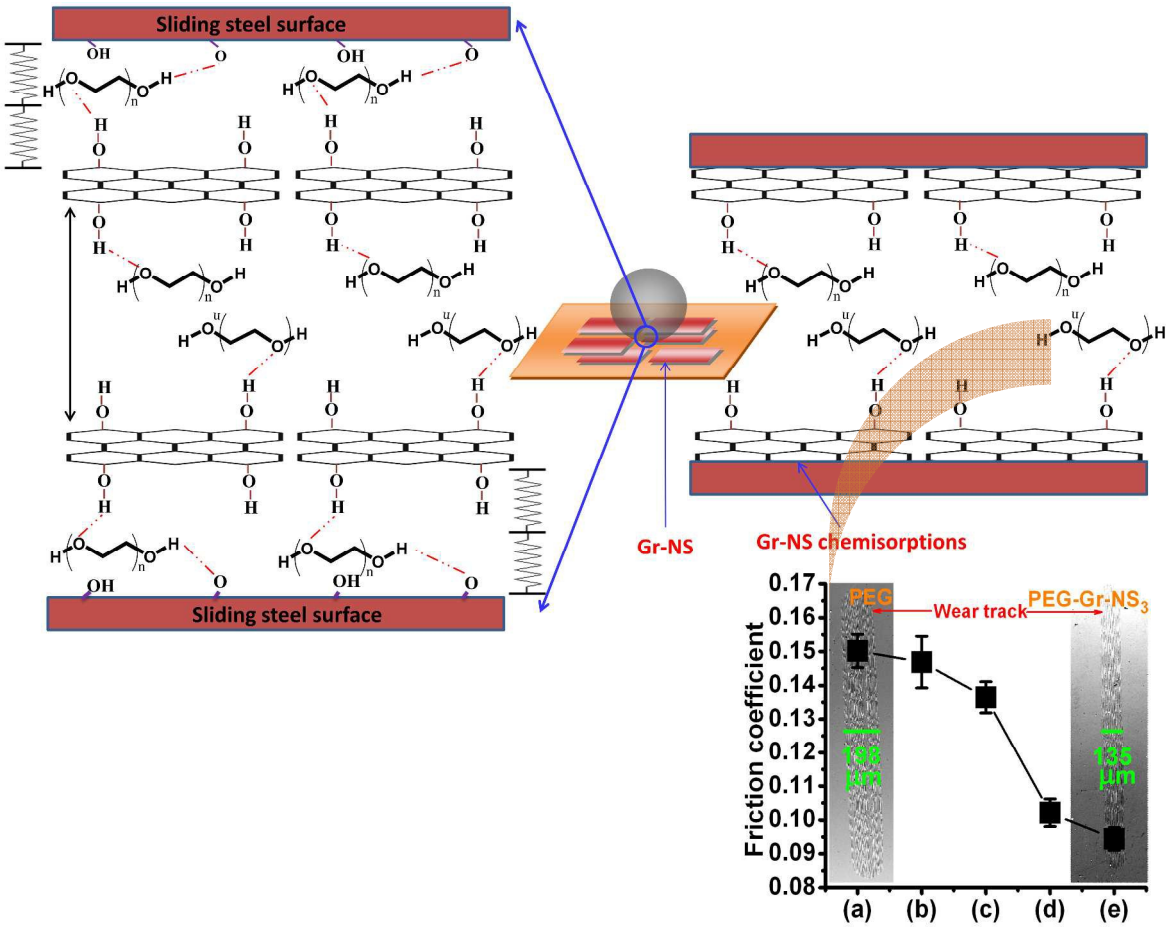


The γ-radiolysis derived chemical grafting of graphite nanosheets with poly(ethylene-glycol) results remarkable decrease in friction coefficient and significantly enhanced antiwear characteristic of steel-steel sliding interfaces.